

Supporting Information

Table of Contents

I. Total cell elongation rate is proportional to cell length.....	1
II. Mathematical description of the cell geometry and mechanical stresses.....	2
III. Mechanical stress in a curved rod-shaped cell and corresponding deviation from the circular cross-section.....	3
1. Perpendicular stress	6
2. Deviation from the circular cross-section.....	7
3. Parallel stress	8
IV. Mathematical relationship between the straightening coefficient S and the processivity of the glycan strand synthesis.....	10
V. Estimating the processivity of the synthesis machinery from the published experimental data.....	13
References.....	16

I. Total cell elongation rate is proportional to cell length

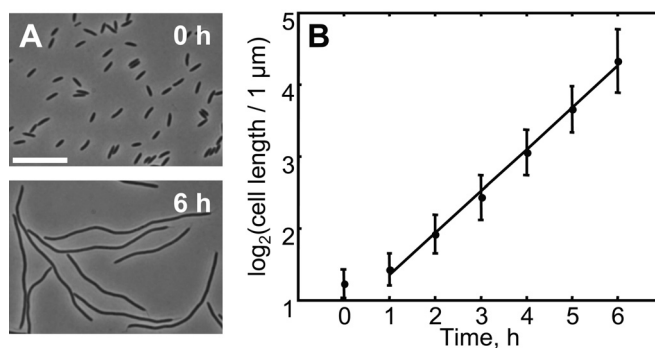


Fig. S1. Growth of non-dividing *C. crescentus* cells. After growth in PYE medium containing xylose at 30°C, CJW1819 cell populations (CB15N $\Delta creS ftsZ::pBJM1$) were synchronized and swarmer cells were transferred to pre-warmed PYE medium containing glucose instead of xylose to stop the expression of the cell division gene *ftsZ* (1). Cells were then grown in a liquid culture at 30°C in a rotary shaker. Aliquots were taken every hour and placed on agarose pads for immediate phase contrast microscopy imaging. **A.** Sample images of the cells at the beginning and at the end of the experiment. Bar: 10 μm . **B.** Plot of the mean cell length in the population as a function of time since synchrony. Note that the initial lag corresponds to recovery after the cold shock produced by synchrony. Error bars indicate the standard deviation of the cell sizes in the population. The length of the cells increases exponentially, indicating proportionality of the growth rate to the cell length. One representative experiment out of 3 is shown; 5608 cells were analyzed in this experiment.

II. Mathematical description of the cell geometry and mechanical stresses

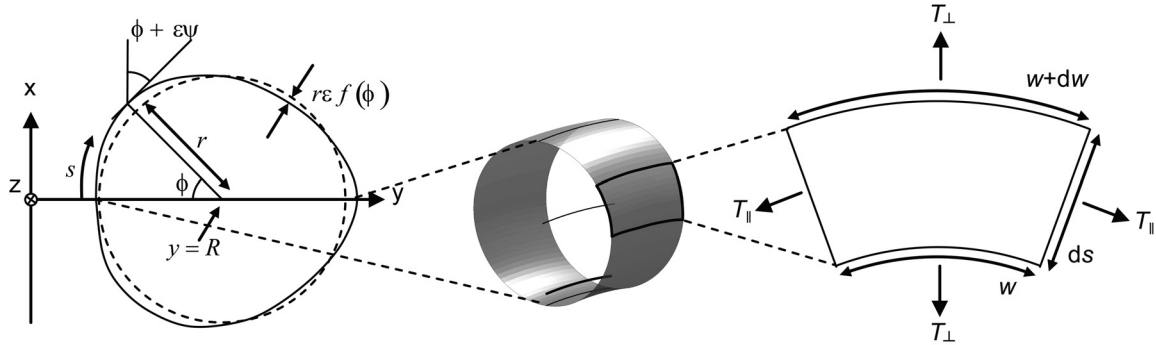


Fig. S2. Description of the cell geometry and definition of the mathematical symbols.

For the purpose of this study, we approximate the cell wall geometry of a curved rod-shaped bacterium as a section of a torus of constant centerline curvature and nearly circular cross-section of constant diameter. In each point of the centerline we define a local Cartesian coordinate system with the origin at the center of the torus and coordinate x pointing perpendicularly to the plane that contains the centerline of the cell. The coordinate y points outward along the direction of the radius of curvature of the cell and intersects the centerline of the cell at the local surface point being considered. The coordinate z is perpendicular to the xy plane such that the z direction is parallel to the tangent to the centerline of the cell (**Fig. S2**). The y axis intersects the cell surface in two points. We will refer to the surface intersection point with larger y coordinate as “outer” and the other as “inner”. Within this framework, the cell shape is characterized by only two parameters: the radius of the cross-section r , which does not change during growth and is considered a property of the bacterial strain and of the environmental conditions, and the radius of the centerline R , which may change during growth.

In reality the toroidal shape is only an approximation: a young short (swarmer) *C. crescentus* cell has a variable cross-sectional diameter, being thinner near the poles, and its shape can only roughly be described as having a constant diameter. Because of the high turgor pressure and the low resistance of the PG to bending and shearing, most of the elastic force in the cell wall comes from stretching deformations. Therefore, turgor pressure is almost entirely opposed by the tension times the curvature of the wall along the two principal axes. Due to its much smaller curvature, the contribution of the stress parallel to the main axis of the cell is much smaller than that in the cell cross section. As a result, the cell cross-section is nearly circular. More exactly, the deviation from the circular shape scales as $O(\varepsilon^2)$, where ε is the ratio between the radius of curvature r of the perpendicular cross section (xy -plane) and the radius of curvature R of the centerline

(i.e. $\varepsilon = r / R$; for the proof, see section III below). Thus, ε can be considered zero for cell curvatures that are small compared to the inverse radius of the cell's cross-section. For example, this is the case for wild-type *C. crescentus* cells, for which $r \approx 0.25 \mu\text{m}$ and $R \approx 2.5 \mu\text{m}$ (2), yielding $\varepsilon = 0.1$ and $\varepsilon^2 = 0.01$. In order not to obscure our model with non-essential details, in our calculations we neglect the small dependence of the straightening mechanism with respect to small deviations in the cell radius along the length of the cell.

To describe mechanical stresses and growth rates, consider a thin segment of a bacterium between two planes perpendicular to the centerline located symmetrically around the xy plane (**Fig. 2B** and **Fig. S2**). If the cell length is significantly longer than its width, we can consider only one such segment from translational symmetry (or rotational symmetry around the x axis). We also define the ‘‘parallel’’ stress T_{\parallel} as the component of the mechanical surface stress in the direction parallel to the cell axis direction (z -direction in the xy plane), and the ‘‘perpendicular’’ stress T_{\perp} as the mechanical surface stress along the cell wall in the plane perpendicular to the centerline (xy -plane at $z=0$).

In this study we consider the growth anisotropic, i.e. a rod-shaped cell grows along its body while keeping the diameter constant. Data suggest that this behavior involves the use of MreB protein (3) and may be achieved by prestretching glycan strands being incorporated (4), though here it is sufficient to simply postulate this behavior without going into the underlying details.

III. Obtaining the straightening coefficient from experimental data

Here we derive the approximate law of curvature decay that we use to fit our crescentin disruption experiments. In the following we assume first that all crescentin filaments get disrupted instantaneously. In a second part of this derivation we make a correction to take into account the initial period during which crescentin structures are still intact in some of the cells. Equation [2] in the main text implies that the curvature of a cell declines exponentially as $C(t) = C_i e^{-t/\tau}$, with C_i being the initial curvature of this cell and τ the decay time. For simplicity, we assume that the initial distribution of the curvature of the free cells (i.e. cells in liquid culture) is Gaussian with mean C_0 and standard deviation σ_0 , i.e.

$$\rho_{ini}(C) = \frac{1}{\sqrt{2\pi} \sigma_0} \exp\left(-\frac{(C - C_0)^2}{2\sigma_0^2}\right), \quad C \in (-\infty, \infty). \quad [\text{S1}]$$

We also assume that the decay rate of the curvature is the same for all cells. As a consequence of these two assumptions the time-dependent distribution $\rho_s(C,t)$ of curvature remains Gaussian for all time with mean and standard deviation that varies according to $C_m(t) = C_0 e^{-\frac{t}{\tau}}$, $t \in [0, \infty)$ and $\sigma_s(t) = \sigma C_m / C_0$, respectively. When the free cells are placed on agarose-padded slides, an additional curvature is added to each cell, which is also assumed to be Gaussian-distributed with zero mean and standard deviation σ_r , and independent of the original curvature of the cell.

$$\rho_r(C) = \frac{1}{\sqrt{2\pi} \sigma_r} \exp\left(-\frac{C^2}{2\sigma_r^2}\right), \quad C \in (-\infty, \infty). \quad [\text{S2}]$$

Thus, the distribution of curvature of the cells on a pad is a convolution of the two mentioned distributions, which is easy to compute for the case of two independent Gaussian distributions:

$$\rho_c(C,t) = \rho_s(C,t) \otimes \rho_r(C) = \frac{1}{\sqrt{2\pi} \sigma} \exp\left(-\frac{(C-C_m)^2}{2\sigma^2}\right), \quad C \in (-\infty, \infty). \quad [\text{S3}]$$

where $C_m(t) = C_0 e^{-\frac{t}{\tau}}$ as previously and $\sigma(t) = \sqrt{\sigma_r^2 + \sigma_s(t)^2} = \sqrt{\sigma_r^2 + \sigma_0^2 (C_m / C_0)^2}$. Note that only the absolute values of the curvature can be measured, so the values of negative curvature (i.e. a cell curved in the opposite direction) will be detected as their absolute values. Thus, the distribution becomes:

$$\rho(C,t) \quad \rho_c(C,t) \quad \rho_c(|C|,t)$$

In order to incorporate the effect of non-simultaneous crescentin structure disruption in different cells we consider the probability density as a sum of probability densities of multiple subpopulations, in each of which the disruption happened at the same moment, different for different subpopulations. Thus, the size of the subpopulation disrupted at the moment t is $-\frac{dn}{dt}(t)$, where $n(t)$ – experimentally measured fraction of the cells with intact crescentin structure. The probability density to have particular curvature C at a given time t becomes

$$\rho_{\Sigma}(C, t) = -\int_0^{\infty} \rho(C, t-t') \frac{dn}{dt}(t') dt'. \quad [S5]$$

In practice, only a few points of $n(t)$ are known, thus for fitting purposes this integral can be approximated by a simple sum of several terms:

$$\rho_{\Sigma}(C, t) = \rho(C, t-t_0)(1-n_0) + \sum_{i=1}^2 \rho\left(C, t - \frac{t_{i-1}+t_i}{2}\right)(n_{i-1} - n_i), \quad [S6]$$

where $t_i = i$ h after the beginning of experiment.

In order to fit the data we used the Maximum Likelihood Estimation method (5). To do so, for each value of data (C_i, t_i) the probability was calculated that the curvature between C_i and $C_i + dC$ (dC is an infinitely small constant) can be obtained at the given time point t_i given the parameters C_m, C_0, σ, τ . The likelihood, or the probability that each point was calculated given the parameters, is the product of these probabilities:

$$\mathcal{L}(C_0, C_m, \sigma, \tau) = \prod_i \rho_{\Sigma}(C_i, t_i | C_0, C_m, \sigma, \tau) \quad [S7]$$

The maximum likelihood is determined as the value of the parameters, at which the likelihood reaches maximum. For practical reasons, however, we maximized the logarithmic likelihood function:

$$\Lambda(C_0, C_m, \sigma, \tau) = \ln \mathcal{L}(C_0, C_m, \sigma, \tau) = \sum_i \ln \rho_{\Sigma}(C_i, t_i | C_0, C_m, \sigma, \tau). \quad [S8]$$

IV. Mechanical stress in a curved rod-shaped cell and corresponding deviation from the circular cross-section

1. Perpendicular stress

Consider the equilibrium of a small curved segment of the cell surface with two boundaries parallel to the centerline ($x=const$ planes) and the other two boundaries in two perpendicular cross-sections located symmetrically around the xy -plane (**Fig. S2, Right**). We will use the perturbation method considering a straight cell as the zero order approximation and using the ratio of the cross-section and the centerline radii $\varepsilon = r/R$ as the small parameter. Denote with w and $w+dw$ the lengths of the segment borders along the surface in the planes $x=const$, and with s the surface arc length in the planes perpendicular to the centerline. The projections of the forces acting on the segment onto its tangential plane consist of the force on its lower (on the figure) boundary $wT_{\perp}(s)$, the force on its upper boundary $(w+dw)T_{\perp}(s+ds)$, and the projection $\sin(\phi+\varepsilon\psi)\frac{w}{y}dsT_{\parallel}(s)$ of the forces acting on the sides $dsT_{\parallel}(s)$. For the later the projection onto the y axis gives the factor w/y and the subsequent projection onto the plane tangential to the surface gives the factor $\sin(\phi+\varepsilon\psi)$. The stresses in the perpendicular and parallel directions, $T_{\perp}(s)$ and $T_{\parallel}(s)$, as well as w , dw , s , ds , and the angles ϕ , and ψ are shown on **Fig. S2**. Because the segment is not moving, these forces are in equilibrium:

$$(w+dw)T_{\perp}(s+ds) = wT_{\perp}(s) + \sin(\phi+\varepsilon\psi)wT_{\parallel}(s)\frac{ds}{y}. \quad [\text{S9}]$$

Now we divide both sides of the equation by $w dy$ to obtain an expression for the derivative of perpendicular stress. On the next step we rewrite the resulting right-hand side only keeping the terms linear in ε (if written in terms of r and T_{\parallel} , T_{\perp}), remembering that $dw/dy = w/y$, $dy/ds = \sin(\phi+\varepsilon\psi)$ and $y = R(1+O(\varepsilon))$:

$$\frac{dT_{\perp}}{dy} = \frac{T_{\perp}(s+ds) - T_{\perp}(s)}{dy} = -T_{\perp} \frac{1}{w} \frac{dw}{dy} + T_{\parallel} \frac{1}{y} \sin(\phi+\varepsilon\psi) \frac{ds}{dy} = \frac{T_{\parallel} - T_{\perp}}{R}. \quad [\text{S10}]$$

Note that in for a straight cell $T_{\perp} = 2T_{\parallel}$ because the equilibrium of forces in the xz plane requires that the pressure P be compensated by the parallel stress force as $\pi r^2 P = 2\pi r T_{\parallel}$. Similarly, the equilibrium in the yz plane requires that the pressure force on a segment of length dy is compensated by perpendicular stress force $2r dy P = 2dy T_{\perp}$. Thus, we have $T_{\perp} = rP = 2T_{\parallel}$ (see also (6)). The same would be true for a curved cell to zero order in ε . Now we go back to the equation [S10], integrate it and rewrite in terms of $\xi = (y - R)/r$. We get:

$$T_{\perp} = T_{\perp 0} - \frac{T_{\perp 0}}{2} \varepsilon \xi + O(\varepsilon^2). \quad [\text{S11}]$$

Here $T_{\perp 0}$ and later $T_{\parallel 0}$ are the values of perpendicular T_{\perp} and parallel T_{\parallel} stresses, respectively, at the centerline $y = R$.

2. Deviation from the circular cross-section

We describe the shape of the cross-section with the angle ϕ and the distance from the center $r \cdot (1 + \varepsilon f(\phi))$ (see **Fig. S2**, *Left*) and write the equation of force balance, this time along the normal to the surface.

$$P = C_{\perp} T_{\perp} - C_{\parallel} T_{\parallel} \cos(\phi + \varepsilon \psi). \quad [\text{S12}]$$

Now we rewrite the curvatures C in terms of inverses of length variables: $C_{\perp} = 1/(r + r\varepsilon f''(\phi))$ and $C_{\parallel} = 1/y$ where $f''(\phi)$ represents the second derivative of f . Substituting into the expression for P together with the expansions of T_{\perp} (see above) and T_{\parallel} to first order in ε ($T_{\parallel} = T_{\parallel 0} + \varepsilon \alpha \xi$ with α a constant) we obtain:

$$P = \frac{1}{r + r\varepsilon f''} \left(T_{\perp 0} - \frac{T_{\perp 0}}{2} \varepsilon \xi \right) - \frac{1}{y} (T_{\parallel 0} + \varepsilon \alpha \xi) \cos(\phi + \varepsilon \psi). \quad [\text{S13}]$$

Keeping only the contributions from the zero and first order in ε and remembering that $1/R = \varepsilon/r$, we get:

$$P = \frac{1}{r}(1 - \varepsilon f'')T_{\perp 0} \left(1 - \frac{\varepsilon \xi}{2}\right) - \frac{1}{R}(1 - \varepsilon \xi)(T_{\parallel 0} + \alpha \varepsilon \xi)(\cos \phi - \varepsilon \psi \sin \phi), \quad [\text{S14}]$$

and finally:

$$P = \frac{T_{\perp 0}}{r} - \varepsilon f'' \frac{T_{\perp 0}}{r} - \varepsilon \xi \frac{T_{\perp 0}}{2r} - \varepsilon \frac{T_{\parallel 0}}{r} \cos \phi. \quad [\text{S15}]$$

Considering the equation [S15] to zero order in ε we have $P = T_{\perp 0} / r$. Considering the equation [S15] to first order in ε and using the relations $T_{\parallel 0} = T_{\perp 0} / 2$ and $\xi = -\cos \phi (1 + \varepsilon r f')$ we obtain that f'' must be zero to zero order in ε :

$$f'' = 0. \quad [\text{S16}]$$

Integrating twice in ϕ we get $f(\phi) = c_1 \phi + c_2$ where c_1 and c_2 are two integration constants. Because f is a symmetric function that is zero at $\phi = 0$, we obtain that

$$f(\phi) = 0 \quad [\text{S17}]$$

to zero order in ε .

3. Parallel stress

Consider the stress at the intersection of the cell surface and the xy plane. From the symmetry of the problem with respect to the yz plane, the stress on the surface can be expressed as a function of y only. Note, that the extension of the cell wall material due to turgor pressure is relatively small, reaching about 17 % for *E. coli* (7), as compared to the maximum strain that the PG can withstand, which is about 300 % (8). As for the majority of systems under relatively small strain, we therefore consider that local deformations are linear with respect to stresses and follows Hook's law, thus providing the linearity of the strain vs. stress dependence to the whole system. Mathematically this linearity can be expressed as T_{\parallel} being a linear function of y : $T_{\parallel} = T_{\parallel 0} (1 + g \cdot (y - R))$. Here g is a constant coefficient. From the equilibrium of the moments due to the parallel stress and the pressure around the x axis we can write

$$\int (y-R) T_{\parallel} ds = \int (y-R) P dA, \quad [\text{S18}]$$

where dA is an area element of the cross-section. Now we substitute the value for T_{\parallel} and the approximations to first order in ε for the area element $dA = r^2 (1/2 + \varepsilon f) d\phi$ and the arc length element $ds = r d\phi$. The equation [S18] becomes:

$$\int_0^{2\pi} (y-R) T_{\parallel 0} (1 + g \cdot (y-R)) r d\phi = \int_0^{2\pi} (y-R) P r^2 (1/2 + \varepsilon f) d\phi. \quad [\text{S19}]$$

In a straight cell, the symmetry of the geometry implies that T_{\parallel} does not depend on ϕ and we have

$$\int_0^{2\pi} (y-R) T_{\parallel 0} r d\phi = \frac{1}{2} \int_0^{2\pi} (y-R) r^2 P d\phi. \quad [\text{S20}]$$

Subtracting the equation [S20] from [S19] we obtain:

$$T_{\parallel 0} g \int_0^{2\pi} (y-R)^2 d\phi = P r \varepsilon \int_0^{2\pi} (y-R) f d\phi. \quad [\text{S21}]$$

In the previous section we derived that $f = O(\varepsilon)$ (equation [S17]), which makes the right hand side no more than of the order of ε^2 . Thus this is also true for the left hand side, i.e. $\int g \cdot (y-R)^2 d\phi = O(\varepsilon^2)$, which is achievable only if $g = O(\varepsilon^2)$. Hence $T_{\parallel} = T_{\parallel 0} + O(\varepsilon^2)$, the parallel stress has no correction in the first order in ε .

V. Mathematical relationship between the straightening coefficient S and the processivity of the glycan strand synthesis.

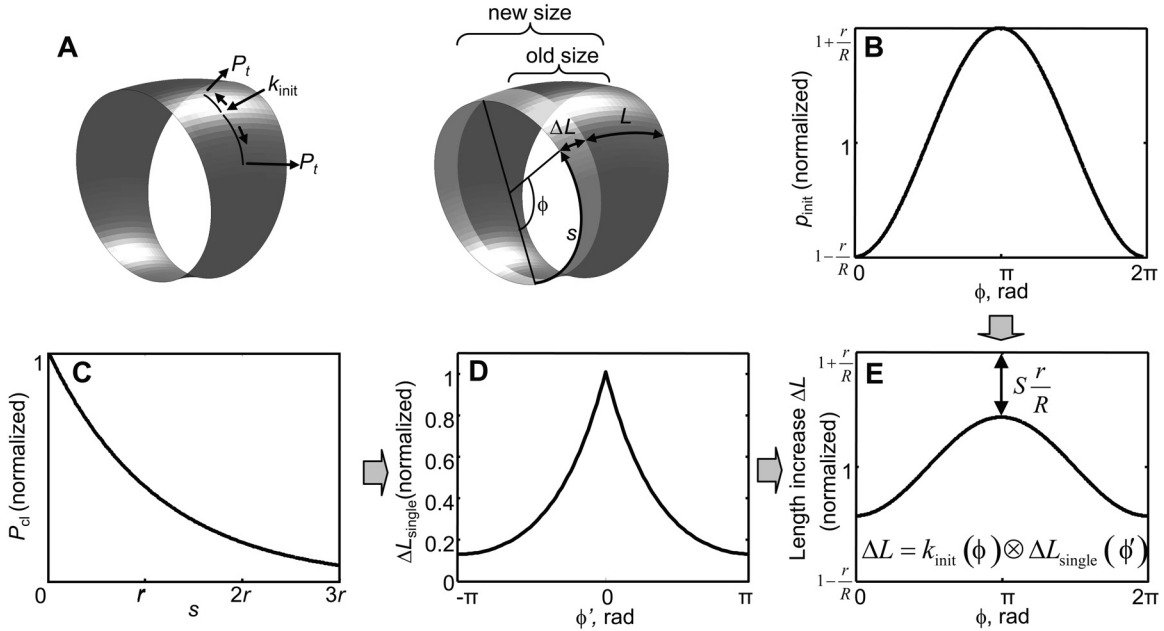


Fig. S3. Relationship between the straightening coefficient and the processivity of PG synthesis. The model assumes a constant probability to initiate synthesis k_{init} per unit area and a constant termination rate P_t per unit length of the synthesized glycan chain. **A.** The geometry of the model. **B-E.** Individual steps in the calculation of the straightening coefficient. **B.** Normalized probability of synthesis initiation as a function of the position on the circumference, $p_{\text{init}}(\phi)$. **C.** Probability density function of the length of the synthesized chains, $p_{\text{cl}}(s)$. **D.** The increment to the length in the z direction per initiation event, $\Delta L_{\text{single}}^+(\phi)$. **E.** The increment to the length in the z direction per unit time, $\Delta L(\phi)$. See the text for the definitions of the mentioned variables. The numerical values of the parameters used to produce the figures are as fitted for the experimental data.

We computed the straightening coefficient as a function of the processivity of the PG synthesis machinery under the following assumptions, justified in the main text: (a) Glycan strands are oriented perpendicularly to the main axis of the cell. In real cells we expect deviations from the perpendicular orientation, but these should only slightly increase the computed value of the processivity. (b) The rate of synthesis initiation per unit area k_{init} is uniform over the cell surface. (c) After initiation, synthesis proceeds in either direction perpendicular to the cell axis. (d) The probability per unit length of the synthesized glycan strand to terminate the synthesis, P_t , is constant.

In a curved cell, the pole-to-pole material lines on the outer side of the cell are longer than on the inner side. Therefore the probability to initiate synthesis will be larger on the outer side of a curved cell because of the difference in the existing length of the segment. More precisely, the infinitesimal surface area on a small toroidal segment (**Fig. 2B** and **Fig. S3A**) centered on the xy plane is $\left(1 - \frac{r}{R} \cos \phi\right) d\bar{L} r d\phi$ where $d\bar{L}$ is the infinitesimal width of the segment averaged over the cross section, which is the same as the infinitesimal length along the centerline. Here $\phi = s / 2\pi r$ is the angular coordinate along the circumference (**Fig. S3B**). Thus, the probability per unit time and unit length along the center line of the cell to initiate synthesis between ϕ and $\phi + d\phi$ is:

$$p_{\text{init}}(\phi) d\phi = k_{\text{init}} \left(1 - \frac{r}{R} \cos \phi\right) r d\phi. \quad [\text{S22}]$$

From the assumption (d), constant probability of synthesis termination, we obtain an exponential distribution for the length of the synthesized chains with the probability density function $p_{\text{cl}}(s) = \exp(-s/s_0)/s_0$ (**Fig. S3C**). Here $s > 0$ and the mean chain length is $s_0 = 1/P_t$.

The next step is to calculate the average amount of material $\Delta L_{\text{single}}(s)$ that is added in the z direction (main axis direction) per initiation event as a function of s , assuming that synthesis starts at some given point along the periphery. Without loss of generality we can choose that point to be $s = 0$. We calculate the cumulative distribution of $p_{\text{cl}}(s)$ and take into account that strands that are longer than the circumference of the cell contribute more than once to the elongation of the cell at a given s . First, we consider only the synthesis that proceeds in the positive s direction:

$$\begin{aligned} \Delta L_{\text{single}}^+(s) &= \frac{\Delta L_0}{2} \sum_{k=0}^{\infty} \int_s^{\infty} p_{\text{cl}}(s' + 2\pi r k) ds' \\ &= \frac{\Delta L_0}{2} \sum_{k=0}^{\infty} \exp\left(-\frac{s + 2\pi r k}{s_0}\right), \quad [\text{S23}] \\ &= \frac{\Delta L_0}{2} \frac{e^{-s/s_0}}{1 - e^{-2\pi r/s_0}} \end{aligned}$$

where $s \in [0, 2\pi r]$ and ΔL_0 is the width of one PG insert (equal to the width of 2 strands for the three-for-one model, where 3 strands get inserted and one gets removed; the value

however can be different if the three-for-one model is not correct). The factor $\frac{1}{2}$ comes from the fact that the two orientations of the synthesis direction are equally probable with the probability $1/2$ each. Rewriting in terms of $\phi \equiv s/r$ and now taking into account synthesis in the other direction we finally obtain:

$$\Delta L_{\text{single}}(\phi) = \Delta L_{\text{single}}^+(\phi) + \Delta L_{\text{single}}^+(2\pi - \phi) = \frac{\Delta L_0}{2} \frac{e^{-\frac{\phi}{\phi_0}} + e^{\frac{\phi-2\pi}{\phi_0}}}{1 - e^{-\frac{2\pi}{\phi_0}}}, \text{ with } \phi \in [0, 2\pi]. \quad [\text{S24}]$$

Taking into account both the initiation and termination of the synthesis, we can finally calculate the rate of growth of the cell in the direction of the centerline as a function of ϕ by convolving the initiation probability per unit time and length $p_i(\phi)$ with the average amount of material $\Delta L_{\text{single}}(\phi)$ contributed by a single initiation event

$$\begin{aligned} \frac{1}{\bar{L}} \frac{\Delta L}{\Delta t} &= p_{\text{init}}(\phi) \otimes \Delta L_{\text{single}}(\phi) = \int_{\phi-2\pi}^{\phi} p_{\text{init}}(\phi') \Delta L_{\text{single}}(\phi - \phi') d\phi' \\ &= \frac{\Delta L_0 r k_{\text{init}}}{2} \int_{\phi-2\pi}^{\phi} \left(1 - \frac{r}{R} \cos \phi'\right) \frac{e^{-\frac{(\phi-\phi')}{\phi_0}} + e^{\frac{\phi-\phi'-2\pi}{\phi_0}}}{1 - e^{-\frac{2\pi}{\phi_0}}} d\phi' \quad . \quad [\text{S25}] \\ &= k_{\text{init}} \Delta L_0 r \phi_0 \left(1 - \frac{1}{1 + \phi_0^2} \frac{r}{R} \cos \phi\right) \end{aligned}$$

On the other hand, from equation [1] in the main text and the facts that $L_1 = \bar{L}(1 + r/R)$ and $L - \bar{L} = -(L_1 - \bar{L}) \cos \phi$ we have

$$\begin{aligned} \frac{1}{\bar{L}} \frac{dL}{dt} &= \frac{d\bar{L}}{\bar{L} dt} - \frac{1}{\bar{L}} \left(\frac{dL_1}{dt} - \frac{d\bar{L}}{dt} \right) \cos \phi = A \left(1 - \frac{1}{\bar{L}} (L_1(1-S) + \bar{L}S - \bar{L}) \cos \phi \right) = \\ &= A \left(1 - (1-S) \frac{L_1 - \bar{L}}{\bar{L}} \cos \phi \right) = A \left(1 - (1-S) \frac{r}{R} \cos \phi \right), \quad [\text{S26}] \end{aligned}$$

Comparing equations [S25] and [S26] we obtain equation [4] in the main text

$$\begin{cases} A = k_{\text{init}} \Delta L_0 r \phi_0 = k_{\text{init}} \Delta L_0 s_0 \\ S = \frac{\phi_0^2}{1 + \phi_0^2} = \frac{s_0^2}{r^2 + s_0^2} \end{cases} \quad [\text{S27}]$$

This result establishes a direct connection between the processivity of the PG synthesis s_0 and the straightening coefficient S . The functional form is a sigmoidal function with Hill coefficient 2 and half max processivity reached at the radius of the cross-section r (**Fig. 3E**). For processivities much smaller than the radius r , the straightening coefficient increases quadratically with the processivity, i.e. $S \propto (s_0 / r)^2$. On the other hand, for processivities much larger than the radius r , the straightening coefficient asymptotically tends to 1. In intermediate cases when s_0 is of the order of r , the straightening coefficient will be of order $S \sim 0.5$.

VI. Estimating the processivity of the synthesis machinery from the published experimental data

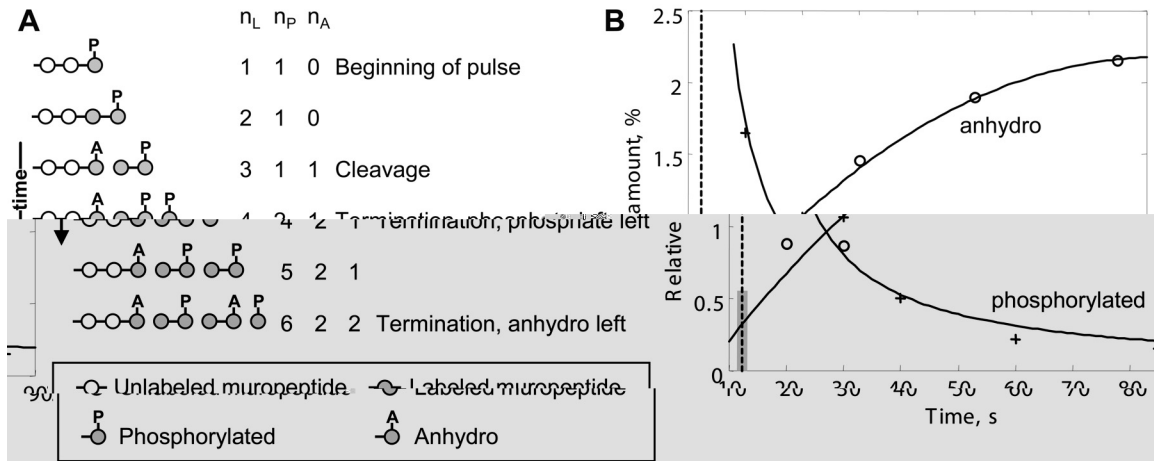


Fig. S4. Measuring processivity from pulse experiments in (9). **A.** Schematics of the process with the different muropeptide species considered in the text. The process is shown per single synthesis point (always on the right) with time increasing in steps required to synthesize a single subunit. **B.** The percentage of glycan chain termini as determined using a pulse experiment (replotted from (9)). Crosses: phosphorylated muropeptides, open circles: 1,6-anhydro ends. A hyperbolic fit is shown for the phosphorylated muropeptides $n_P / n_L = n_P / s(t - t_S)$ with offset $t_S \approx 11.4$ s, providing an estimate for the diaminopimelic acid intake time. A spline fit is shown for the anhydro ends, providing the estimates for the value at the offset time ($t = 11.9$ s, dashed line) of 0.30 %.

PG is made of glycan strands crosslinked by short peptides. Its subunit consists of a disaccharide of *N*-acetylglucosamine and *N*-acetylmuramic acid bound to a peptide chain,

containing among other amino acids an unusual one, diaminopimelic acid (A_2pm), in the amount of one molecule per subunit (reviewed in (10)). For our purpose PG synthesis can be summarized into five processes: (a) initiation of glycan strand synthesis; (b) elongation by addition of new subunits to the growing strands by transglycosylation reactions (11, 12) (reviewed in (3)); (c) incorporation of new strands (possibly 3 at a time according to the 3-to-1 model (13)) into the PG by crosslinking to existing strands via peptide bonding; (d) termination of strand synthesis; and (e) cleavage of incorporated glycan strands. Importantly, some of the mentioned processes may occur concurrently on the same strand.

The transglycosylation reaction is mediated by penicillin-binding proteins (PBPs), which processively add new monomers to existing strands (14). Based on the high processivity of the reaction observed *in vitro* (14), we expect that a glycan strand continues growing until the catalytic enzyme dissociates. Therefore, there will be an average length of newly synthesized glycan strands that is set by the PBP binding affinity. (Formally, there is also the possibility that a glycan strand could be cleaved between the bound PBP and the first crosslink, effectively causing PBP dissociation from the PG.) In this work we define *processivity* as the mean number of subunits incorporated into a glycan chain from the initiation to the termination of elongation process, when the chain (or 3 chains, in the three-for-one model) cannot be extended further. Thus, within this framework processivity is equal to the inverse of the probability of termination per subunit synthesized (or relative termination rate). In what follows, we use data from pulse experiments done on *E. coli* (9) to estimate the value of the processivity.

Note that our definition of processivity is equivalent to the traditional one, defined as the number of subunits added by a single PBP performing the synthesis from the initiation to the termination. The processivity is longer than the mean mature length of glycan chains because the latter are cleaved by lytic transglycosylases after, and possibly even during, synthesis (15).

The subunit at the growing end of a glycan strand is phosphorylated (9). In addition, the prevalent view is that in Gram-negative species, glycan chain ends in mature PG are modified to form 1,6-anhydromuramic acid (16, 17), which can be formed when a glycan chain is cleaved by a lytic transglycosylase (18). It is less clear, however, whether the end subunit remains phosphorylated after termination of glycan strand synthesis or if termination effectively results in the terminal subunit modified with an anhydro group (10, 16). For completeness, we will assume that termination can leave either a phosphate or an anhydro group, though one of these two may never happen – in which case its rate is zero (**Fig. S4A**). Therefore, measuring the fraction of phosphorylated subunits in the PG gives the number of polymerizing ends plus some fraction of the number of terminated ends. Likewise, measuring the fraction of anhydro groups as a function of

time gives information on the cleavage and termination rates. The time courses for both of these fractions have been measured using pulse and pulse-chase experiments with [^3H]A₂pm labeling the subunits (9).

To estimate the rate at which termination leaves a phosphorylated subunit, we consider that there are two possible sources of phosphorylated ends—actively growing strands and terminated ends. During the pulse with label, the number of actively growing ends is constant per cell surface unit, and all are labeled. Note that deviations from this rule because of cell curvature can be considered small and are neglected here. The number of terminated, phosphorylated ends is also constant per cell surface unit, but the fraction that is labeled is proportional to the fraction of the PG that is labeled. At early time points following the start of the pulse, only a very small fraction of the PG is labeled. Therefore, the labeled phosphorylated fraction is dominated by actively growing ends. As time passes and the fraction of the PG that is labeled increases, terminated ends begin to dominate the labeled and phosphorylated fraction. Here we assume that the phosphate does not get removed enzymatically after synthesis because no suitable enzyme for this purpose is known (19). At long time points, the labeled phosphorylated fraction is completely dominated by terminated ends, as the fraction of labeled growing ends becomes negligible. Therefore, the fraction of labeled phosphorylated ends at these points yields the probability of termination per subunit incorporation event. From the long time behavior in the data (Fig. 2C in (9) replotted in **Fig. S4B**) we determine that less than 0.15% of the labeled subunits are phosphorylated, and this fraction may be as small as zero.

Next we determined the probability of termination per subunit synthesized yielding an anhydro-modified end. These ends can be produced by either termination or cleavage. Just as with phosphorylated ends, the fraction of labeled anhydro ends produced by termination is proportional to the fraction of PG that is labeled. However, because cleavage continues after glycan strand incorporation, the chance that any subunit will be cleaved and anhydro-modified increases with time. Thus, at early time points after the beginning of the label pulse, it is more likely that a labeled anhydro end is a product of termination than cleavage. We use a spline fit to extrapolate to a short time the fraction of labeled anhydro groups that was measured as a function of time by Glauner and Höltje (Fig. 2C in (9) replotted in **Fig. S4B**). We extrapolate to a time of about 11 s in order to allow for uptake of the labeled subunits as estimated from fitting the fraction of phosphorylated subunits. This time is also adequate for a newly synthesized glycan strand to be incorporated (estimated to be <1 s with a glycan synthesis rate of 9 subunits/s and 6 subunits/crosslink (9)). From this analysis, we find that the anhydro end-producing termination rate per subunit synthesized to be between zero and an upper bound of 0.55%

(grey zone on the vertical dashed line in Fig. S3B), with the estimated value from the extrapolation at 0.30%.

The total termination probability per subunit synthesized is then estimated as 0.30 % with lower and upper bounds 0 and $0.15 + 0.55 = 0.7$ %, respectively. Note that the precision of the extrapolation is not sufficient to exclude the possibility that either the anhydro end-producing termination rate or the phosphate end-producing rate might be zero. In **Fig. S4B** these two cases would correspond to the fit to the circles (crosses) tending to zero at the origin (infinity), respectively. For this reason this analysis cannot provide a lower bound higher than zero for the total termination probability per subunit synthesized. The upper bound however is unaffected by these considerations.

The inverse of this value yields an estimate for the processivity of PG synthesis in *E. coli* of about 337 subunits, with a lower bound at 142 subunits. This number significantly exceeds the mean length of glycan chain in mature PG, which was found to be 31 subunits in the same work (9). Cleavage of the glycan strands after incorporation most likely accounts for this discrepancy. A value of 337 subunits for the processivity in *E. coli* is consistent with the value of the processivity (279 subunits) that we found for *C. crescentus* in order to explain the rate of straightening observed in our experiments.

References

1. Kelly AJ, Sackett MJ, Din N, Quardokus E, & Brun YV (1998) Cell cycle-dependent transcriptional and proteolytic regulation of FtsZ in *Caulobacter*. *Genes Dev* 12(6):880-893.
2. Cabeen MT, *et al.* (2009) Bacterial cell curvature through mechanical control of cell growth. *Embo J* 28(9):1208-1219.
3. Vollmer W & Bertsche U (2008) Murein (peptidoglycan) structure, architecture and biosynthesis in *Escherichia coli*. *Biochim Biophys Acta* 1778(9):1714-1734.
4. Lan G, Wolgemuth CW, & Sun SX (2007) Z-ring force and cell shape during division in rod-like bacteria. *Proc Natl Acad Sci U S A* 104(41):16110-16115.
5. Edwards AWF (1972) *Likelihood* (Cambridge University Press) 1st Ed.
6. Koch AL (1988) Biophysics of bacterial walls viewed as stress-bearing fabric. *Microbiol Rev* 52(3):337-353.
7. Koch AL, Lane SL, Miller JA, & Nickens DG (1987) Contraction of filaments of *Escherichia coli* after disruption of cell membrane by detergent. *J Bacteriol* 169(5):1979-1984.
8. Koch AL & Woeste S (1992) Elasticity of the sacculus of *Escherichia coli*. *J Bacteriol* 174(14):4811-4819.
9. Glauner B & Hölte J-V (1990) Growth pattern of the murein sacculus of *Escherichia coli*. *The Journal of Biological Chemistry* 265(31):18988-18996.
10. Vollmer W (2008) Structural variation in the glycan strands of bacterial peptidoglycan. *FEMS Microbiol Rev* 32(2):287-306.

11. Ward JB & Perkins HR (1973) The direction of glycan synthesis in a bacterial peptidoglycan. *Biochem J* 135(4):721-728.
12. van Heijenoort J (2001) Formation of the glycan chains in the synthesis of bacterial peptidoglycan. *Glycobiology* 11(3):25R-36R.
13. Holtje J-V (1993) Three for one - a simple mechanism that guarantees a precise copy of the thin, rod-shaped sacculus of *Escherichia coli*. *Bacterial Growth and Lysis: Metabolism and Structure of the Bacterial Sacculus*, eds de Pedro MA, Holtje J-V, & Löffelhardt W (Plenum Press, New York), pp 419-426.
14. Yuan Y, *et al.* (2007) Crystal structure of a peptidoglycan glycosyltransferase suggests a model for processive glycan chain synthesis. *Proc Natl Acad Sci U S A* 104(13):5348-5353.
15. Scheurwater E, Reid CW, & Clarke AJ (2008) Lytic transglycosylases: bacterial space-making autolysins. *Int J Biochem Cell Biol* 40(4):586-591.
16. Vollmer W, Blanot D, & de Pedro MA (2008) Peptidoglycan structure and architecture. *FEMS Microbiol Rev* 32(2):149-167.
17. Vollmer W & Seligman SJ (2010) Architecture of peptidoglycan: more data and more models. *Trends Microbiol* 18(2):59-66.
18. Höltje JV, Mirelman D, Sharon N, & Schwarz U (1975) Novel type of murein transglycosylase in *Escherichia coli*. *J Bacteriol* 124:1067-1076.
19. Vollmer W, Joris B, Charlier P, & Foster S (2008) Bacterial peptidoglycan (murein) hydrolases. *FEMS Microbiol Rev* 32(2):259-286.